3D SIMULATION OF FLAPPING FLAGS IN A UNIFORM FLOW BY THE IMMERSED BOUNDARY METHOD

Wei-Xi Huang[1] and Hyung Jin Sung[*2]

We present an immersed boundary (IB) method for 3D simulation of flappingflags in a uniform flow. The proposed formulation is manipulated on the basis of an efficient Navier-Stokes solver adopting the fractional step method and a staggered Cartesian grid system. A direct numerical method is developed to calculate the flag motion, with the elastic force treated implicitly. The fluid motion defined on an Eulerian grid and the flag motion defined on a Lagrangian grid are independently solved and the mass of flag is handled in a natural way. An additional momentum forcing is formulated from the flag motion equation in a way similar with the direct-forcing IB formulation and acts as the interaction force between the flag and ambient fluid. A series of numerical tests are performed and the present results are compared qualitatively and quantitatively with previous studies. The instantaneous flag motion is analyzed under different conditions and surrounding vortical structures are identified. The effects of physical parameters on the flapping frequency are studied.

Key Words : Immersed boundary method, Fluid-structure interaction, Flapping flag, Direct-forcing

1. INTRODUCTION

The flapping of flags in wind is a commonplace and familiar phenomenon in everyday life, but still puzzles people due to its extremely complicated dynamics. The flapping dynamics is also essential in the tail or wing motions of swimming and flying animals. For a passively flapping flag, it exerts inertial and elastic forces on the fluid, while the fluid acts on the flag through pressure and viscosity. Together, these interactions between the fluid and the flag can give rise to self-sustained oscillations at its natural frequencies. Even for active biological swimming and flight, the frequency of the tail or wing flapping cannot be selected arbitrarily[1]. Recent researches revealed a simple relationship between the flapping frequency, amplitude and forward speed for a wide range of species of animals to fly or swim at high propulsive efficiency[2-4]. Hence, the study of flapping dynamics is helpful to understand such biological processes.

Fluid structure interactions like the flag-in-wind problem are challenging to numerical simulation on account of their complex geometries and freely moving boundaries. Recently, several immersed boundary (IB) methods have been developed for simulating fluid-structure interactions. Among these methods, the IB method developed by Peskin[5] has its advantage in dealing with two-way coupling interactions by an efficient transform between Eulerian and Lagrangian variables. However, the boundary is usually considered to be massless or neutrally buoyant in previous IB methods. In our work aimed at simulating flexible filaments in a fluid as in Zhang et al.'s experiment[6], we proposed a different formulation to handle the mass of a filament in a natural way[7].

So far, direct simulations have been carried out for the interactions between 2D fluid flow and flexible filaments or plates using various methods, including the IB method [7,8]. However, few numerical results on 3D flags flapping in a viscous fluid flow have been available in

1 학생회원, 한국과학기술원 기계공학과
2 정회원, 한국과학기술원 기계공학과
* Corresponding author, E-mail: hjsung@kaist.ac.kr

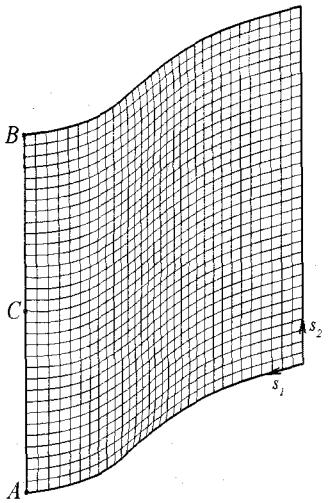

Fig. 1 Schematic diagram of the Lagrangian grid system and its curvilinear coordinates (s_1, s_2) on the flag surface.

literatures. Kim and Peskin[9] simulated 3D flag-in-wind problem using their penalty immersed boundary method, but no details of numerical discretization about the 3D flag model was described and results were reported briefly in their paper. In the present study, we extend our previous work to the 3D simulation of flapping flags in a uniform flow, manipulated in the frame of IB formulation. Problem formulation is described in the next section and numerical method is introduced in Section 3. We present numerical results in Section 4. Finally, a summary is given in Section 5.

2. PROBLEM FORMULATION

The flag motion is described by Lagrangian variables. A curvilinear coordinate system (s_1, s_2) is attached to the flag surface, as shown in Fig. 1. Among the four boundaries, one is fixed at $s_1 = 0$ while the other three are free boundaries. The longitudinal coordinate s_1 ranges from 0 to L, and the latitudinal coordinate s_2 ranges from 0 to H, where L and H denote the length and width of the flag, respectively. Here we neglect the flagpole to keep the symmetry of geometry about $s_2 = H/2$. The direction of the gravity force is along the s_2-axis, which breaks the symmetry about $s_2 = H/2$ and causes the flag to sag down.

The non-dimensional form of the flag motion equation can be written as

$$\frac{\partial^2 \boldsymbol{X}}{\partial t^2} = \sum_{i,j=1}^{2} \left[\frac{\partial}{\partial s_i} \left(\sigma_{ij} \frac{\partial \boldsymbol{X}}{\partial s_j} \right) - \frac{\partial^2}{\partial s_i \partial s_j} \left(\gamma_{ij} \frac{\partial^2 \boldsymbol{X}}{\partial s_i \partial s_j} \right) \right] + Fr \frac{\boldsymbol{g}}{g} - \boldsymbol{F} \tag{1}$$

where $\boldsymbol{X}(s_1, s_2, t)$ denote the Cartesian coordinates of an arbitrary point on the flag surface, σ_{ij} denote the stretching and shearing coefficients, γ_{ij} denote the bending and twisting coefficients, $\boldsymbol{g}$ denotes the gravity force with $g = |\boldsymbol{g}|$, and $\boldsymbol{F}$ denotes the Lagrangian forcing exerted on the filament by the surrounding fluid. In Eq.(1), Fr is Froude number defined as $Fr = gL_r / U_\infty^2$ where L_r denotes the characteristic length, and $\sigma_{ij} = \phi_{ij}\left(T_{ij} - T_{ij}^0\right)$ with $T_{ij} = \frac{\partial \boldsymbol{X}}{\partial s_i} \cdot \frac{\partial \boldsymbol{X}}{\partial s_j}$. At the fixed boundary, we use the simply-supported condition, i.e.

$$\boldsymbol{X} = (0, 0, s_2), \frac{\partial^2 X}{\partial s_1^2} = 0, at\ s_1 = 0. \tag{2}$$

At the free boundaries, we have

$$\frac{\partial^2 X}{\partial s_1^2} = 0, \frac{\partial^3 X}{\partial s_1^3} = 0, at\ s_1 = L, \tag{3}$$

$$\frac{\partial^2 X}{\partial s_2^2} = 0, \frac{\partial^3 X}{\partial s_2^3} = 0, at\ s_2 = 0 \text{ or } H, \tag{4}$$

and

$$\sigma_{ij} = 0, \gamma_{ij} = 0 \quad (i, j = 1, 2) \tag{5}$$

The non-dimensional governing equations for the incompressible fluid flow are

$$\frac{D\boldsymbol{u}}{Dt} = -\nabla p + \frac{1}{Re} \nabla^2 \boldsymbol{u} + \boldsymbol{f} \tag{6}$$

$$\nabla \cdot \boldsymbol{u} = 0 \tag{7}$$

where $\boldsymbol{u} = (u, v, w)$ is the velocity vector, p is the pressure, $Re = \rho_0 U_\infty L_r / \mu$ is the Reynolds number with ρ_0 the fluid density and μ the dynamic viscosity, and $\boldsymbol{f}$ is the momentum forcing applied to enforce the no-slip boundary condition along the IB. Note that we use different characteristic densities, i.e. the fluid density ρ_0 and the flag density ρ_1, in the non-dimensionalization of

Eq.(6) and Eq.(1) respectively. In Eq.(6) the momentum forcing f is scaled by $\rho_0 U_\infty^2/L_r$, while in Eq.(1) the Lagrangian counterpart F is scaled by $\rho_1 U_\infty^2/L_r$. Such difference should be taken into consideration for transformation between the Lagrangian and Eulerian momentum forcings.

In the present study, we evaluate the momentum forcing term at the Lagrangian points directly from the flag motion equation (Eq.(1)). The time-discretized flag motion equation is written as follows:

$$\frac{X^{n+1}-2X^n+X^{n-1}}{\triangle t^2} = RHS^{n+1} - F^n \tag{8}$$

where the superscript n denotes the nth time step, $\triangle t$ denotes the time increment, and RHS regroups the elastic force terms and the gravity force term in Eq.(1) for simplicity. To obtain the desired position of the IB at the next time step, the momentum forcing term can be given by

$$F^n = -\frac{\tilde{X}_{ib}^{n+1}-2X^n+X^{n-1}}{\triangle t^2} + RHS^{n+1} \tag{9}$$

where $\tilde{X}_{ib}^{n+1}$ represents a estimation of the new position of the fluid point, which is initially aligned along the IB. In other words, the momentum forcing in Eq.(9) forces the IB points to move with surrounding fluid points. $\tilde{X}_{ib}^{n+1}$ is estimated by

$$\tilde{X}_{ib}^{n+1} = X_{ib}^n + U_{ib}^n \triangle t \tag{10}$$

where X_{ib}^n is the position of the fluid point at the present time step and U_{ib}^n is the fluid velocity interpolated at the Lagrangian point X^n.

In practice, we found that the coefficient $-1/\triangle t^2$ in Eq.(9) becomes very large since $\triangle t$ is usually given a small value, and one may fail to obtain a stable solution. The first term on the right hand side of Eq.(9) works essentially as a feedback function. Small variation of $\tilde{X}_{ib}^{n+1}$ may cause large change in the term $-\left(\tilde{X}_{ib}^{n+1}-2X^n+X^{n-1}\right)/\triangle t^2$. Hence, we neglect RHS^{n+1} in Eq.(9) and relax the coefficient of the term $-\left(\tilde{X}_{ib}^{n+1}-2X^n+X^{n-1}\right)/\triangle t^2$, i.e.

$$F^n = -\kappa\left(\tilde{X}_{ib}^{n+1}-2X^n+X^{n-1}\right) \tag{11}$$

where κ is a large negative constant. After obtaining the Lagrangian momentum forcing term, we transform it to the Eulerian form by the Dirac delta function

$$f^n(x,t) = \rho\int_\Gamma F^n \delta(x-X)\,ds_1 ds_2 \tag{12}$$

where $\rho = \rho_1/\rho_0 L_r$ comes from non-dimensionalization due to the fact that the Dirac delta function is three-dimensional but there is only two integrals ds_1 and ds_2 in Eq.(12). The difference between the present formulation and those of Peskin's [8,9] is that the flag motion equations are solved independently here, making it possible to dealing with additional constraints on the IB motion easily, such as the mass of the IB.

3. COMPUTATIONAL SCHEME

We use the operator K to represent the discretized form of the elastic force. The discretization of Eq.(1) can be written as

$$\frac{X^{n+1}-2X^n+X^{n-1}}{\triangle t^2} = KX^{n+1} + Fr\frac{g}{g} - F^n + BC \tag{13}$$

where the elastic force term is treated fullly implicitly, the momentum forcing term is calculated by Eq.(11), and the last term BC is the boundary condition vector which contains the known positions at the fixed boundary. After rearrangement, Eq.(13) becomes

$$AX^{n+1} = R^{n+1} \tag{14}$$

where $A = I - \triangle t^2 K$ with I the unit matrix of size $M(N+1)$ and R^n collects all the other terms. To solve Eq.(14), we need to know the initial position and velocity the flag. We found that symmetry and positive-definiteness of the matrix A is preserved in this study. Hence, the conjugate gradient method can be utilized to solve the Eq.(14) in an efficient manner due to its fast convergence rate.

The discretized N-S equations are solved by the fractional step method on a staggered Cartesian grid. The velocity components and momentum forcing are defined on the staggered grid, whereas the pressure is applied at the centers of cells. Fully implicit time advancement is employed, with the Crank-Nicholson scheme being used for the discretization ofthe diffusion and convection terms. Decoupling of the velocity and pressure is achieved by block LU decomposition in conjunction with approximate factorization. Details of the approximate factorization can

be found in Kim et al. [10]. Due to the implicit treatment of the nonlinear convection terms, further decoupling of the intermediate velocity components is made and finally a system of tridiagonal matrices is formed instead of a large sparse matrix. The momentum equation is then solved directly without iteration, and the computational cost is reduced significantly. The pressure Poisson equation is solved by a direct method using FFT or a multigrid method. The pressure is then used to correct the velocity field to satisfy the continuity equation.

The overall process of the present numerical algorithm for simulating the flag motion in a uniform flow is summarized as follows:

(1) At the nth time step, we know the fluid velocity field u^n and the filament position X^n and velocity U^n. Estimate the new position of the fluid point $\tilde{X}_{ib}^{n+1}$ by Eq.(10). Then calculate the Lagrangian momentum forcing F^n by Eq.(11).

(2) Spread the Lagrangian momentum forcing to the Eulerian grid by using Eq.(12). Solve N-S equations to obtain the updated fluid velocity field and pressure field. Interpolate the fluid velocity at the IB to obtain U_{ib}^{n+1} and calculate the new position of the fluid point $X_{ib}^{n+1} = X_{ib}^n + U_{ib}^{n+1}\Delta t$.

(3) Substitute F^n into Eq.(14) and solve this equation to obtain the flag position at the new time step X^{n+1}, as well as the flag velocity $U^{n+1} = (X^{n+1} - X^n)/\Delta t$. This ends one time step marching.

4. RESULTS

In the present simulations, the computational domain for fluid flow is a rectangular box, extending from $(-1,-4,-1)$ to $(7,4,1)$ in the streamwise (x), transverse (y) and spanwise (z) directions, respectively. Here the domain sizes are scaled by the character length L_r. Dirichlet boundary conditions are used at the inflow $(x=-1)$ and far-field boundaries $(y=\pm 4)$, a convective boundary condition is used at the outflow $(x=7)$, and a periodic boundary condition is used in the spanwise direction. A grid size of $513\times151\times129$ is used to discretize the computational domain. The grid mesh is uniformly distributed along the x- and z-axes, while stretched in the y-axis. The fixed boundary of the flag $(s_1=0)$ is aligned with the z-axis, with its midpoint coincided with the origin of the Eulerian coordinate system. The flag surface is discretized by a uniform grid system $\Delta s_1 = \Delta s_2 = 1/64$, which is equivalent to the Eulerian grid spacings Δx, Δy and Δz near the IB.

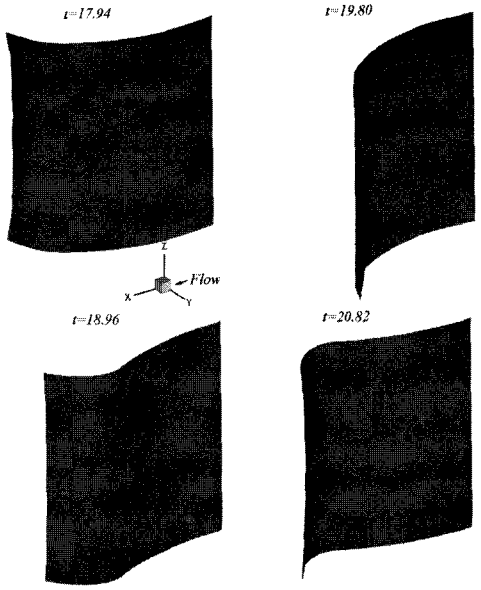

Fig. 2 Instantaneous flag positions in a flapping period at $Re=200$ and $Fr=0$.

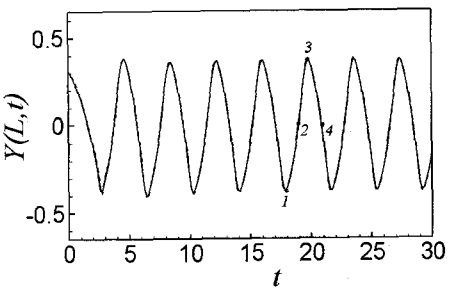

Fig. 3 Time history of the transverse position of the trailing edge of the flag at $Re=200$ and $Fr=0$: ——, point A; ....., point B; -------, point C.

Fig. 2 shows instantaneous flag positions during a flapping period at $Re=200$ and $Fr=0$. Other parameters used here are $L=1.0$, $H=1.0$, $\rho=1.0$, $\phi_{11}=\phi_{22}=1000$, $\phi_{12}=10$ and $\gamma_{11}=\gamma_{22}=\gamma_{12}=0.0001$, which is unchanged in this simulation unless otherwise stated. The four instants used in Fig. 2 are labeled sequentially in Fig. 3, which shows time history of the transverse position of the trailing edge of the flag. The flag is flapping uniformly in the latitudinal (s_2) direction as shown in Fig. 2. As an evidence (Fig. 3), the two corner points and the midpoint of the trailing edge travel

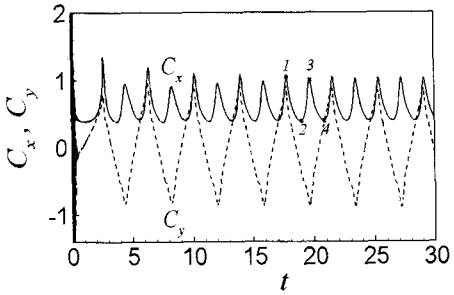

Fig. 4 Time history of the streamwise and transverse drag forcesof the flag at $Re = 200$ and $Fr = 0$.

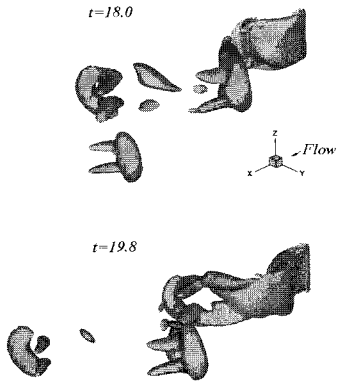

Fig. 5 Vortical structures shedding from the flapping flag at $Re = 200$ and $Fr = 0$.

coincidentally in the transverse direction. Fig.4 displays time history of the streamwise drag force coefficient C_x and the transverse lift force coefficient C_y. It is seen that both C_x and C_y varies periodically with time, while the frequency of the former is twice of that of the latter. This phenomena is similar to that of flow over a circular cylinder[11], since vortical structures shedding from the flag trailing edge at the upper and lower transverse positions both result in the maximum streamwise drag force, but result in the maximum and minimum transverse lift force respectively. Fig. 5 shows 3D instantaneous vortical structures around the flag identified using λ_2 -criterion. We can see a transverse part and two streamwise parts in a vortical structure due to the flapping motion of the trailing edge and the two side edges.

When the Reynolds number is increased to at $Re = 500$ (Fig. 6), small wavy motions are apparent on the flag surface, although the main wave is still travelling along the s_1-direction and uniform in the s_2-direction. Due to increase of the Reynolds number, the vortex rings are formed behind the flag (Fig. 7). Interestingly, the

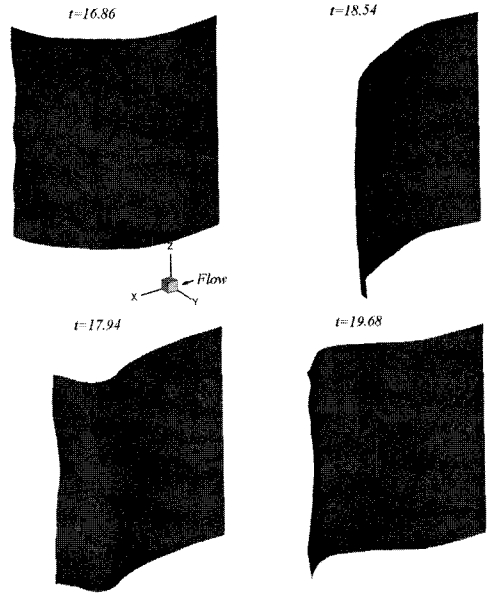

Fig. 6 Instantaneous flag positions in a flapping period at $Re = 500$ and $Fr = 0$.

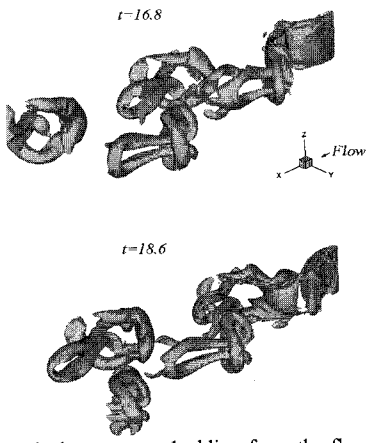

Fig. 7 Vortical structures shedding from the flapping flag at $Re = 500$ and $Fr = 0$.

vortex shedding from the trailing edge forms an O-shape structure, while that from the side edges forms a Ω-shape structure which is connected to the O-shape structure at the bottom.

Now we take into account the effects of the gravity force. The direction of the gravity force is along the spanwise direction, i.e. $g/g = (0,0,-1)$. We use $Re = 500$ and $Fr = 0.2$ in this simulation. Fig .8 shows instantaneous flag positions at four time instants which are also marked in the time history of the transverse position

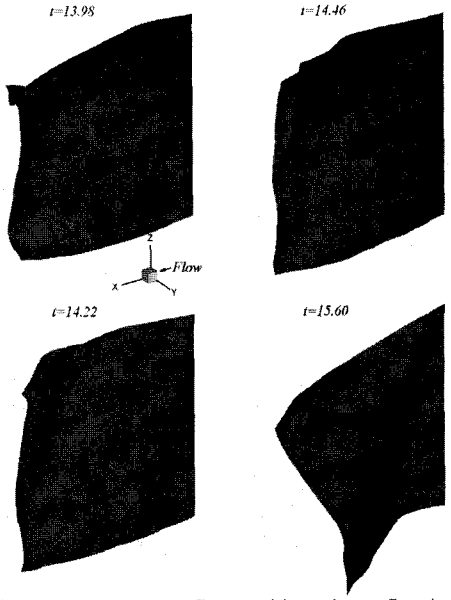

Fig. 8 Instantaneous flag positions in a flapping period at $Re = 500$ and $Fr = 0.2$.

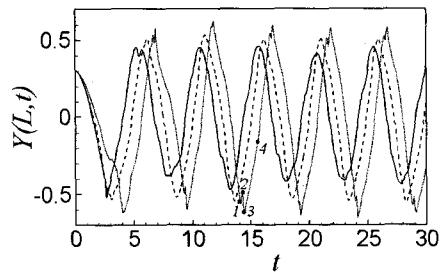

Fig. 9 Time history of the transverse position of the trailing edge of the flag at $Re = 500$ and $Fr = 0.2$: ——, point A; ....., point B; -------, point C.

of the trailing edge (i.e. points 1-4 in Fig. 9). It is clear that the flag is sagging down at $t = 15.60$ as shown in Fig. 8, and Fig. 9 indicates that points A, B and C are travelling out of phase. As a result, the upper corner on the trailing edge experiences a fast rolling near the maximum or minimum transverse positionduring each period, which is shown in Fig. 8 from $t = 13.98$ to $t = 14.46$ as well as in Fig. 9 from point 1 to point 3. Since small wavy motions become apparent and irregular in the flag surface, the streamwise and transverse drag forces (see Fig. 10) are not smooth any more as compared with the case without gravity force (Fig. 4). However, the fundamental frequency of the streamwise drag force is still twice of that of the transverse drag force, indicating the main vortical structure is remaining similar to the case without gravity force. The 3D

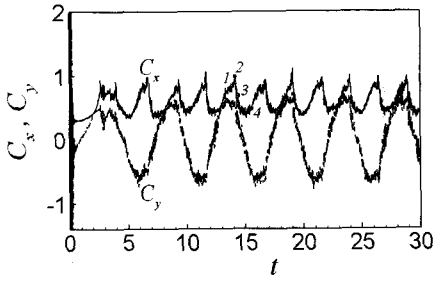

Fig. 10 Time history of the streamwise and transverse drag forces of the flag at $Re = 500$ and $Fr = 0.2$.

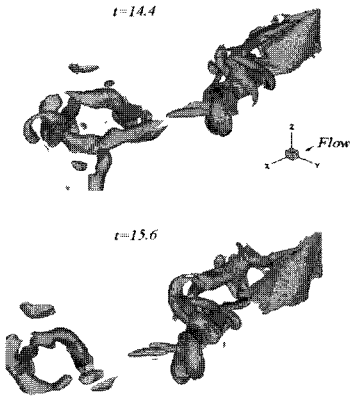

Fig. 11 Vortical structures shedding from the flapping flag at $Re = 500$ and $Fr = 0.2$.

instantaneous vortical structures around the flag are displayed in Fig. 11. The O-shape structures are still evident while the Ω-shape structures are broken due to the sagging-down of the flag and the fast rolling of its upper corner.

The Strouhal number of the flag's flapping at different Reynolds numbers is collected in Fig.12 where we set $Fr = 0$. There are two selections of the length scale for the definition of the Strouhal number. One is the characteristic length L_r which is also used in the definition of Reynolds number; the other is the flapping amplitude A which is measured as the maximum flapping span. Specifically, they are written as $St = fL_r/U_\infty$ and $St' = fA/U_\infty$, respectively, where f denotes the frequency of flapping. As shown in Fig. 12(a), St keeps constant with increasing Reynolds number. Shelley et al.[12] also observed in their experiment that the flapping frequency is proportional to flow speed, which is equivalent to the statement that St is constant. The result indicates that the inertial force is dominant over the viscous force exerted on the flag by its surrounding fluid. In Fig. 12 (a), it is evident that the density has a

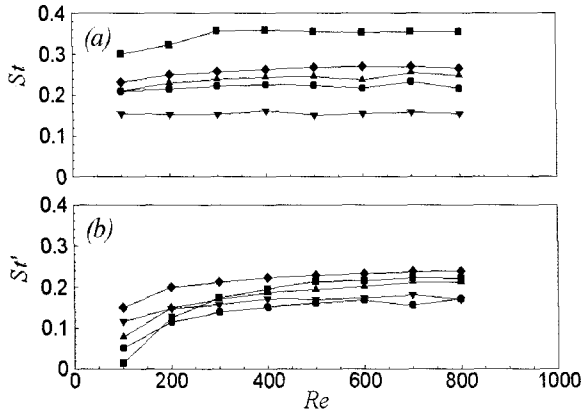

Fig. 12 Strouhal number defined in terms of (a) the length of the flag and (b) the flapping amplitude of the flag as a function of Reynolds number: —■—, $\rho = 0.5$; —▲—, —◆—, —●—, $\rho = 1.0$; —▼—, $\rho = 2.0$. We set $H = 5/8$ and $\gamma_{11} = \gamma_{22} = \gamma_{12} = 0.0001$ for all the cases except that $H = 1$ for —◆— and $\gamma_{11} = \gamma_{22} = \gamma_{12} = 0.001$ for —●—.

significant influence on St, while effects of the flag width and the bending and twisting coefficients are insignificant. However, the difference of St' at different conditions is small, as shown in Fig. 12(b). St' increases slightly with increasing Reynolds number and is between 0.15 and 0.25 for all cases in Fig. 12(b) when $Re \geq 300$. This range is close to the result of Shelley et al.[12], where the reported value is between 0.22 and 0.31. More interestingly, Taylor et al.[3] calculated St' of 42 species of birds, bats and insects in unconfined cruising flight and found that it is constrained in a narrow range $0.2 < St' < 0.4$, as well as swimming dolphins, sharks and bony fish[2]. Especially, birds using direct flight have $St' \approx 0.2$, which is within the range of the present results. This comparison indicates that the active flying and swimming in nature exploit a similar fluid dynamics with that of the passive flapping to obtain high propulsive efficiency.

5. SUMMARY

In the present study, we presented an immersed boundary (IB) method for 3D simulation of flapping flags in a uniform flow, on the basis of an efficient Navier-Stokes solver adopting the fractional step method and a staggered Cartesian grid system. The fluid motion defined on an Eulerian grid and the flagmotion defined on a Lagrangian grid are independently solved. An additional momentum forcing is formulated from the flag motion equation and acts as the interaction force between the flag and ambient fluid. In the present method, the mass of flag is handled naturally and the elastic force is treated implicitly.

A series of numerical tests were performed and the instantaneous flag motion was analyzed under different conditions. The flag flaps uniformly when the gravity force was excluded. An O-shape vortical structure was shedding from the trailing edge, connected by a Ω-shape structure shedding from both side edges. After including the gravity force, the sagging-down motion was evident and the rolling motion of the upper-corner was observed. As a result, the vortical structures were deformed greatly. The Strouhal number defined in terms of the character length L_r was invariant with Reynolds number, indicating that the inertial force is dominant over the viscous force exerted on the flag by its surrounding fluid. If the Strouhal number is defined in terms of the flapping amplitude, it increases slightly with increasing Reynolds number and is between 0.15 and 0.25 when $Re \geq 300$ for all cases, consistent the general value of a flying or swimming animal.

ACKNOWLEDGEMENTS

This work was supported by the Creative Research Initiatives of the Korea Science & Engineering Foundation and partially supported by the Korea Institute of Science and Technology Information under the Strategic Supercomputing Support Program.

REFERENCES

[1] 2000, Wang, Z. J., "Vortex shedding and frequency selection in flapping flight," *J. Fluid. Mech.*, Vol.410, pp.323-341.

[2] 2000, Triantafyllou, M.S. et al., "Hydrodynamics of Fishlike Swimming," *Annu. Rev. Fluid Mech.*, Vol.32, pp.33-53.

[3] 2003, Taylor, G.K. et al., "Flying and swimming animals cruise at a Strouhal number tuned for high power efficiency," *Nature*, Vol.425, pp.707-711.

[4] 2006, Fish, F.E. and Lauder, G.V., "Passive and Active Flow Control by Swimming Fishes and Mammals," *Annu. Rev. Fluid Mech.*, Vol.38, pp.193-224.

[5] 2002, Peskin, C.S., "The immersed boundary method,"

Acta Numerica, pp.479-517.

[6] 2000, Zhang, J. et al., "Flexible filaments in a flowing soap film as a model for one-dimensional flags in a two-dimensional wind," *Nature*, Vol.408, pp.835-839.

[7] 2007, Huang, W.-X. et al., "Simulation of Flexible Filaments in a Uniform Flow by the Immersed Boundary Method," *Journal of Computational Physics*, Vol.226, pp.2206-2228.

[8] 2002, Zhu L. and Peskin, C.S., "Simulation of a Flapping Flexible Filament in a Flowing Soap Film by the Immersed Boundary Method," *Journal of Computational Physics*, Vol.179, pp.452-468.

[9] 2007, Kim Y. and Peskin, C.S., "Penalty Immersed Boundary Method for an Elastic Boundary with Mass," *Physics of Fluids* Vol.19, p.053103.

[10] 2002, Kim, K. et al., "An implicit velocity decoupling procedure for incompressible Navier-Stokes equations," *Int. J. Numer. Meth. Fluids*, Vol.38, pp.125-138.

[11] 2007, Huang, W.-X. and Sung, H. J., "Vortex Shedding from a Circular Cylinder near a Moving Wall," *Journal of Fluids and Structures*, Vol.23, pp.1064-1076.

[12] 2005, Shelley, M. et al., "Heavy Flags Undergo Spontaneous Oscillations in Flowing Water," *Physical Review Letters*, Vol.94, p.094302.